Supplement of Atmos. Chem. Phys., 24, 12055–12077, 2024
https://doi.org/10.5194/acp-24-12055-2024-supplement

Atmospheric Chemistry and Physics
Open Access
EGU

Supplement of

Atmospheric black carbon in the metropolitan area of La Paz and El Alto, Bolivia: concentration levels and emission sources

Valeria Mardoñez-Balderrama et al.
Correspondence to: Valeria Mardoñez-Balderrama (v.mardonez@isac.cnr.it)

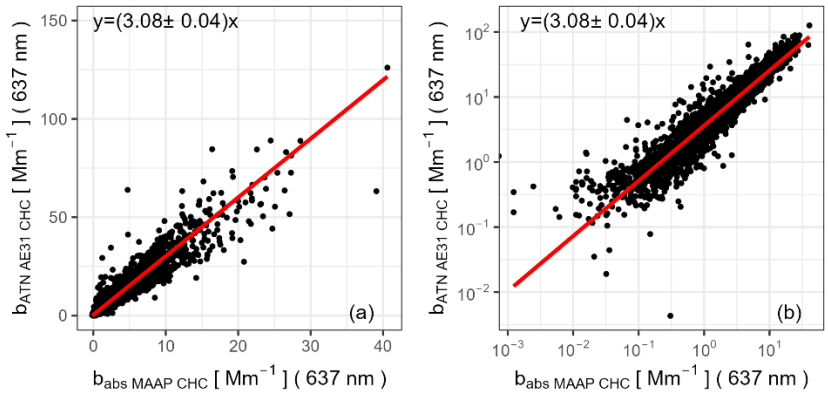

Figure S1. Scatterplot of bATN_AE31(637 nm) vs. babs_MAAP(637 nm) measured between 10 and 16 hours at CHC-GAW between April 2016 and July 2018 in (a) regular and (b) logarithmic scale. The red line represents the Deming fitting line described in the equation displayed on the top-left.

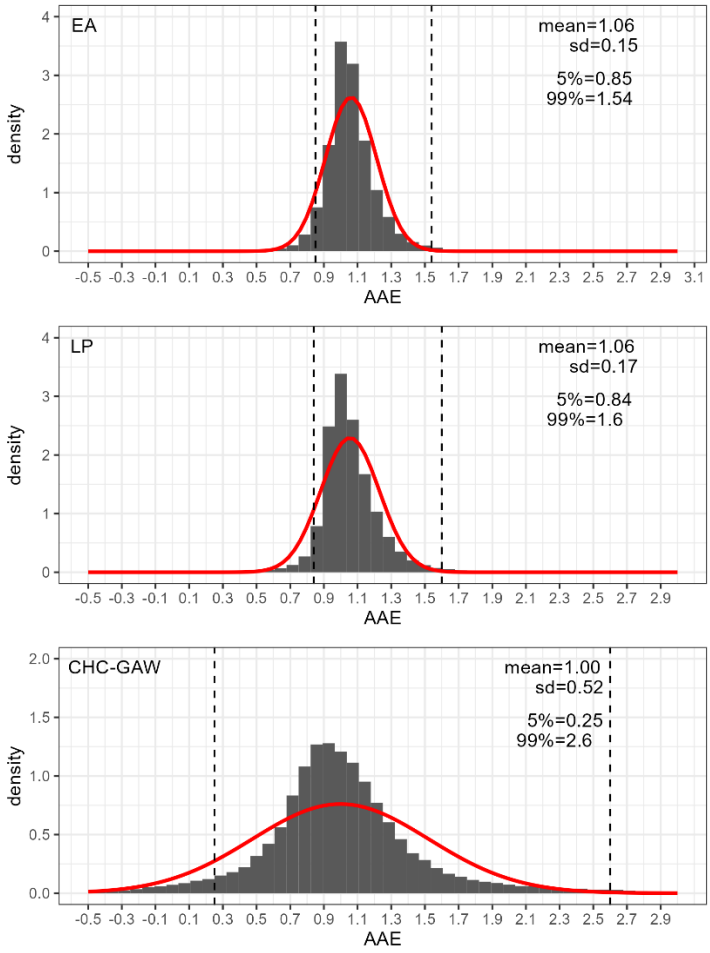

Figure S2. Density distribution of the calculated AAE at the three sampling sites at a 5-min resolution. Red lines represent the fitted normal function and the dashed vertical lines represent the 5% and 99% quintiles. The edges of the of the density distribution beyond the range [-0.5,3] were cut for visual purposes.

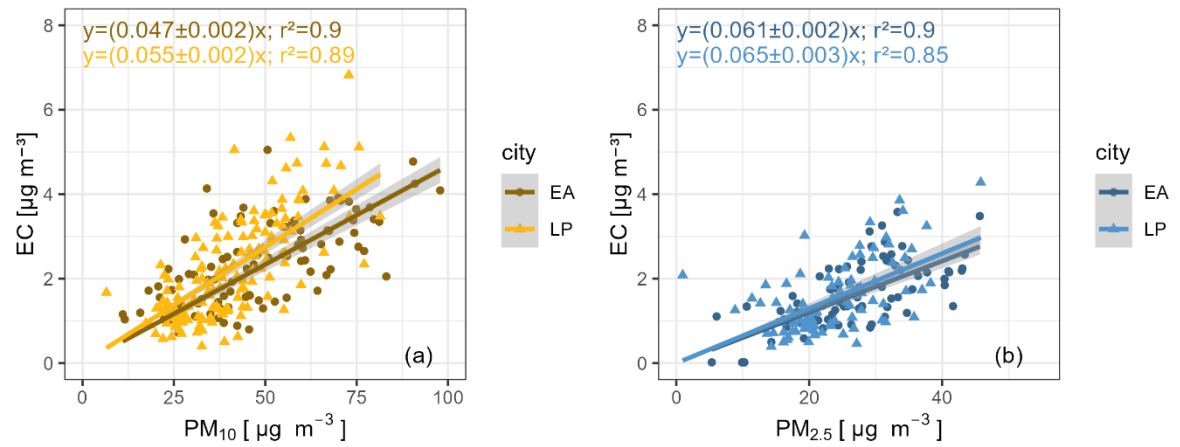

Figure S3. Scatter plot of daily average BC concentrations vs PM_{10} (left panel) and $PM_{2.5}$ concentrations at both sites (right panel). San Juan episodes (June 23-25) were excluded.

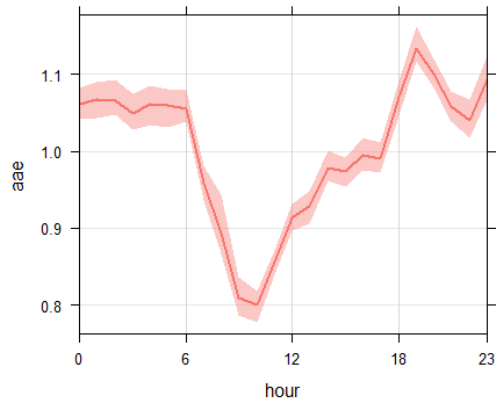

Figure S4. Diurnal variability of AAE in CHC-GAW during the studied period (2016-2018)

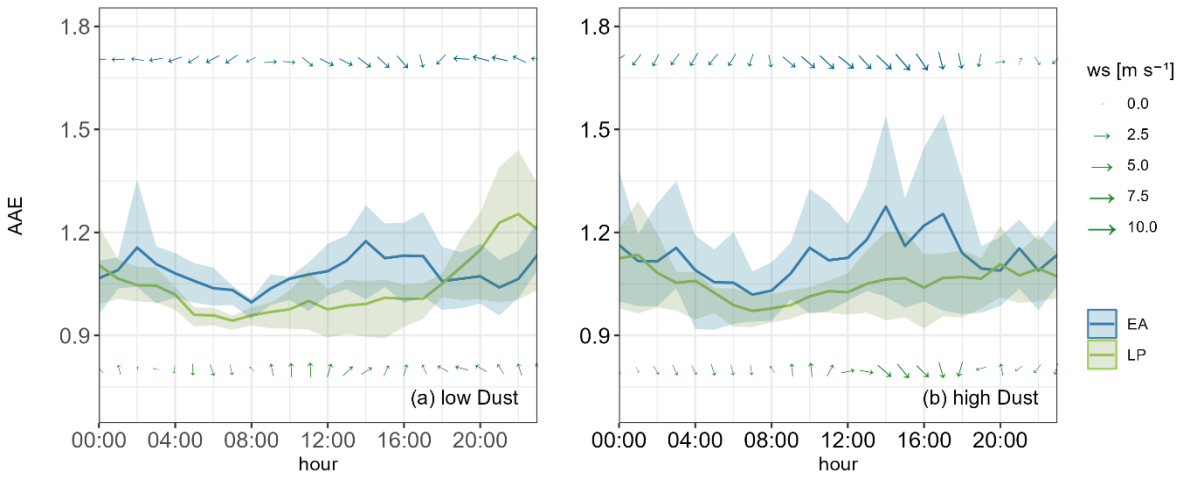

Figure S5. Average diurnal variation of the AAE (solid lines), wind speed and wind direction (arrows above and below the solid lines, the arrowhead points to the direction to which the wind blows) at both sites during (a) low dust episodes and (b) and high dust episodes taken place during the dry season. The shaded area behind the solid curves represents the 25 and 75 percentiles. A low dust episode is considered a day in which the contribution of the dust factor obtained from the source apportionment presented by Mardoñez et al. (2023) is below the percentile 25, per city. Inversely, a high dust episode is defined as the day when the dust contribution exceeded the percentile 75. It can be observed that as expected, High dust events are characterized by higher wind speeds compared to low dust episodes.

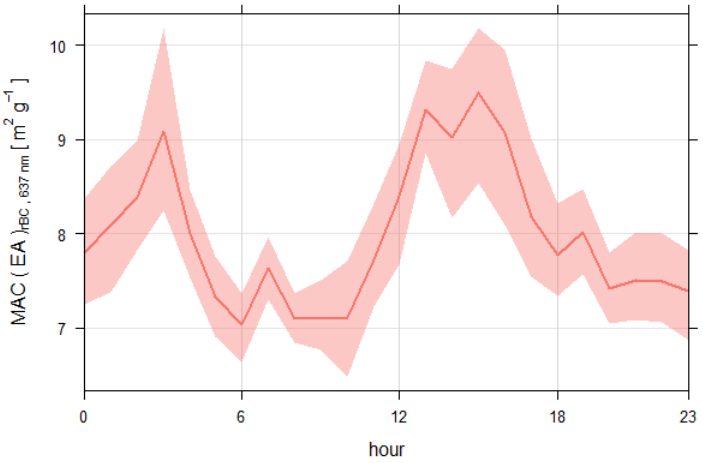

Figure S6. Average diurnal variation of MAC values (solid line) estimated for the city of El Alto. The shaded are represents the 95% confidence interval.

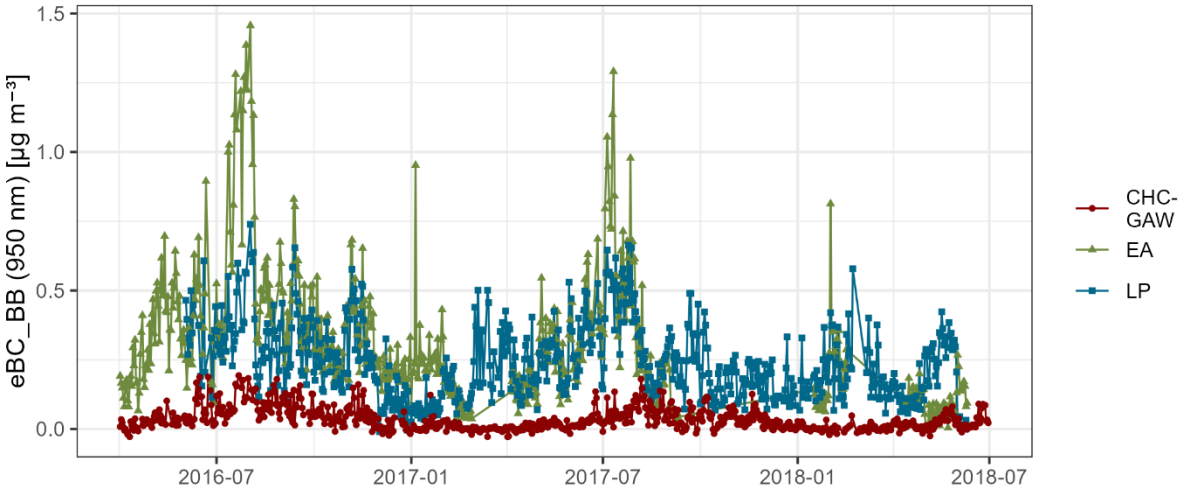

Figure S7. Time series of the BC_{BB} estimated through the Aethalometer method

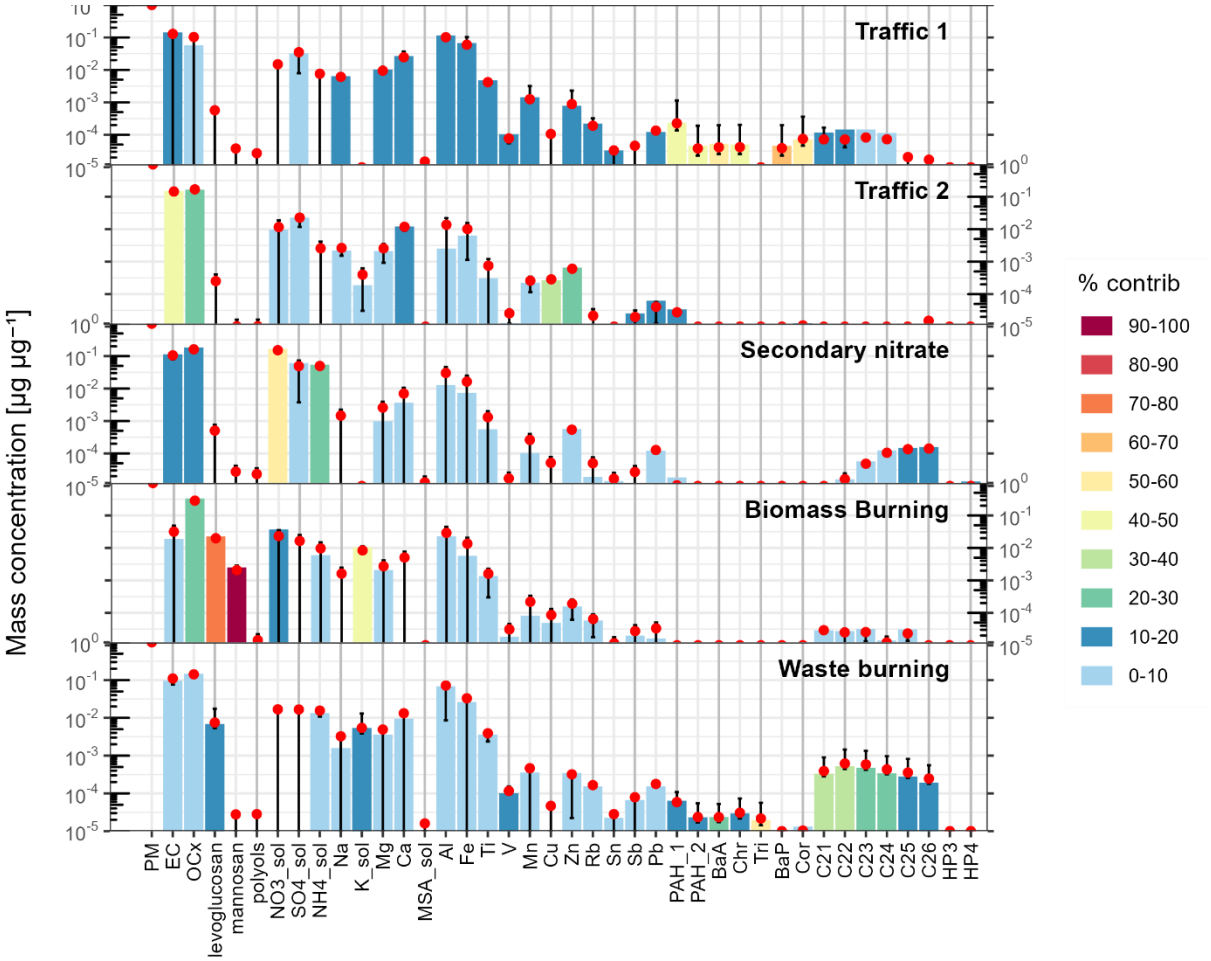

Figure S8. Chemical profiles of the PM_{10} sources resolved by Mardoñez et al., 2023 thorough the PMF analysis, that were included in the multi-linear regression (MLR) analysis performed in the present study to identify the main sources of BC, as described in section 2.5.2 (Image adapted from Mardoñez et al., 2023).

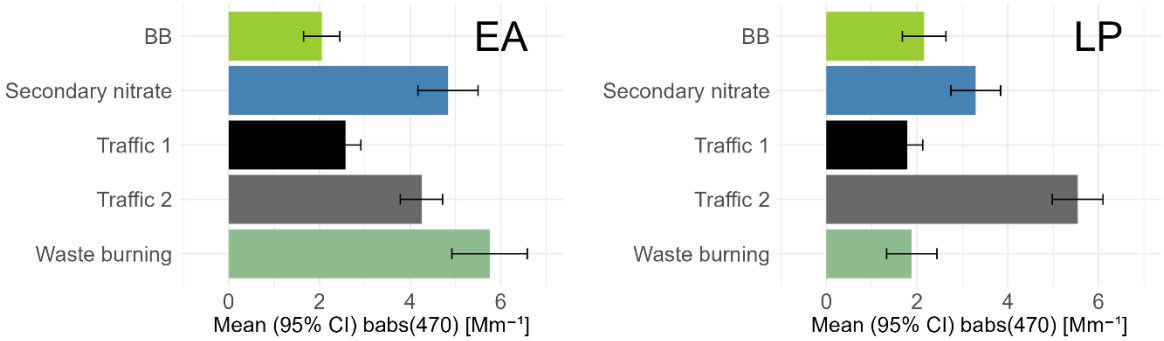

Figure S9. Mean contribution to absorption at a wavelength of 400 nm of the five sources of PM_{10} resolved by Mardoñez et al. (2023) (left: EA, right: LP) that presented a positive contribution to total absorption and a p-value <0.05 in the multilinear ordinary least-squares regression.

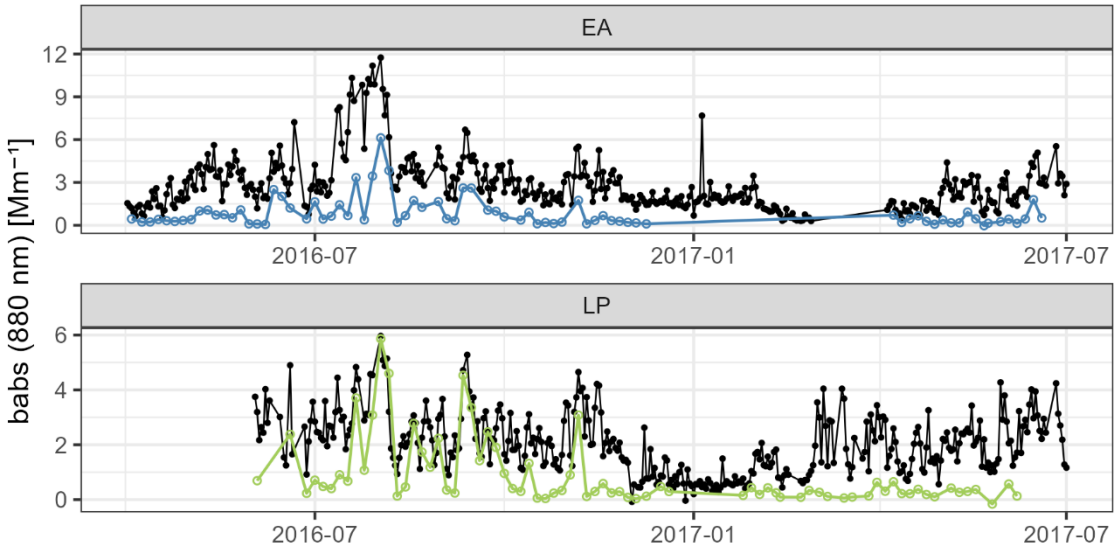

Figure S10. Timeseries of the contribution of agricultural biomass burning to the absorption coefficients measured at the two urban background sites (LP and EA) using two different apportioning methods: Aethalometer method (black lines, with AAE_{TR}=0.85 and AAE_{BB}=1.57) and MLR deconvolution from the mass contribution of PM_{10} sources resolved by Mardoñez et al. (2023) (colored lines).

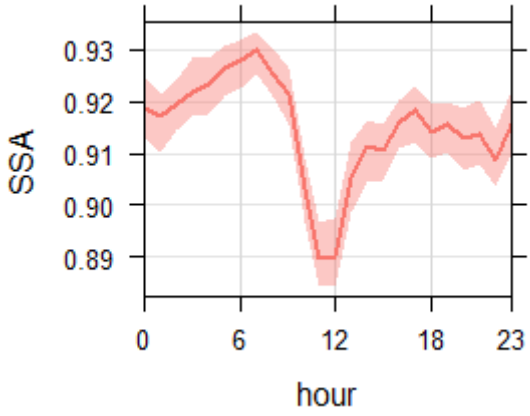

Figure S11. Diurnal variation of single scattering albedo (SSA) in CHC-GAW, calculated as the ratio of the scattering coefficients (measured by a nephelometer Aurora 3000) to the extinction coefficients (scattering+absorption), during the years 2016-2018. The values included in the figure were constrained to the percentiles (1,99) to exclude outliers caused by noise level absorption and scattering coefficients. The shaded area around the solid line represents the 95% confidence interval. The scattering coefficients used to obtain the SSA values displayed in this figure were accessed from EBAS (https://ebas.nilu.no) hosted by NILU. Specifically, the use included data affiliated with the frameworks: ACTRIS, GAW-WDCA.

Table S1. BC vs EC least square linear regression coefficients and their corresponding spearman correlation coefficients

	Intercept [g m^{-3}]	*Slope*	*r (spearman)*
EA_PM_{10}	0.31	0.54	0.80
EA_$PM_{2.5}$	0.32	0.54	0.70
LP_PM_{10}	0.15	0.47	0.90
LP_$PM_{2.5}$	0.21	0.49	0.93
CHC-GAW_PM_{10}	0.07	1.7	0.77

Table S2. Median MACEC and MACrBC calculated following eq. [3] using EC and rBC mass concentrations measured at the three sampling sites. The MAC values were extrapolated to other commonly reported wavelengths using the corresponding daily mean AAEs (with average values of 1.1±0.2 in the urban area and 1.0±0.3 in CHC-GAW).

BC mass		λ [nm]	CHC-GAW[i] Nighttime (23h-8h)	CHC-GAW Daytime (10h-16h)	EA	LP
EC-PM10	MAC_{EC} ± IQR [$m^2 g^{-1}$]	550 nm	24.1±10.8	---	9.1±3.0	6.9±1.7
		637 nm	19.7±9.3	---	7.8±2.5	6.1±1.7
		880 nm	14.0±6.9	---	5.3±1.8	4.1±1.0
EC-PM2.5	MAC_{EC} ± IQR [$m^2 g^{-1}$]	550 nm	---	---	8.6±2.7	8.5±1.9
		637 nm	---	---	7.7±2.0	7.5±1.7
		880 nm	---	---	5.5±1.4	5.0±1.1
SP2-XR (SP2-XX in CHC)	MAC_{rBC} ± IQR [$m^2 g^{-1}$]	550 nm	26.3±8.7	21.8±5.2	8.6±2.2	*10.7±6.0*[ii]
		637 nm	22.7±7.5	18.8±4.5	7.8±2.1	*9.5±5.4*[ii]
		880 nm	16.4±5.4	13.6±3.3	5.6±1.4	*6.7±3.3*[ii]

[i] MAC_{EC} in CHC-GAW are calculated only during night-time periods (23:00-8:00), when the station is outside the influence of the urban mixing layer. MAC_{rBC} in CHC-GAW calculated during the times the station is under the influence of the urban mixing layer (10:00-16:00) between April and May 2018.

[ii]Median MAC_{rBC} in La Paz were calculated for the rBC mass concentrations that resulted from rBC mass-size distributions that peaked above the detection limit of the SP2_XR (i.e. approx. 10% of the cases).

Table S3. Normalized mean EC and OC concentrations contained in the chemical profiles of the sources (Mardoñez et al., 2023) included in the MLR source identification model, The mean concentrations were normalized by the average mass of PM_{10} attributed to each source factor, presented in the last column.

	EC [%]	OC [%]	PM [µg m^{-3}]
TR2	15.2	17.4	4.7
Waste	13.2	19.8	1.3
Sec. Nitrate	11.4	20.0	1.9
TR1	9.8	6.8	2.1
BB	2.8	29.8	2.7

Table S4. Source-specific AAE obtained following the pairwise method used by Zotter et al. (2017).

	AAE (370, 950 nm)	AAE (470, 950 nm)
BB	1.66±0.05	1.52±0.07
NO3	0.97±0.03	0.99±0.04
TR1	1.01±0.07	0.98±0.09
TR2	0.86±0.03	0.88±0.04
Waste	1.10±0.03	1.07±0.04

References

Mardoñez, V., Pandolfi, M., Borlaza, L. J. S., Jaffrezo, J., Alastuey, A., Besombes, J., Moreno R., I., Perez, N., Močnik, G., Ginot, P., Krejci, R., Chrastny, V., Wiedensohler, A., Laj, P., Andrade, M., and Uzu, G.: Source apportionment study on particulate air pollution in two high-altitude Bolivian cities: La Paz and El Alto, Atmos. Chem. Phys., 23, 10325–10347, https://doi.org/10.5194/acp-23-10325-2023, 2023.

Zotter, P., Herich, H., Gysel, M., El-Haddad, I., Zhang, Y., Mocnik, G., Hüglin, C., Baltensperger, U., Szidat, S., and Prévôt, A. S. H.: Evaluation of the absorption Ångström exponents for traffic and wood burning in the Aethalometer-based source apportionment using radiocarbon measurements of ambient aerosol, Atmos. Chem. Phys., 17, 4229–4249, https://doi.org/10.5194/acp-17-4229-2017, 2017.